Acta Mech Sin (2009) 25:787–794
DOI 10.1007/s10409-009-0307-x

RESEARCH PAPER

Numerical investigations of asymmetric flow of a micropolar fluid between two porous disks

Muhammad Ashraf · M. Anwar Kamal · K. S. Syed

Received: 30 November 2007 / Revised: 23 July 2008 / Accepted: 5 June 2009 / Published online: 10 November 2009

Abstract Numerical solution is presented for the two-dimensional flow of a micropolar fluid between two porous coaxial disks of different permeability for a range of Reynolds number Re ($-300 \leq Re < 0$) and permeability parameter A ($1.0 \leq A \leq 2.0$). The main flow is superimposed by the injection at the surfaces of the two disks. Von Karman's similarity transformations are used to reduce the governing equations of motion to a set of non-linear coupled ordinary differential equations (ODEs) in dimensionless form. An algorithm based on the finite difference method is employed to solve these ODEs and Richardson's extrapolation is used to obtain higher order accuracy. The results indicate that the parameters Re and A have a strong influence on the velocity and microrotation profiles, shear stresses at the disks and the position of the viscous/shear layer. The micropolar material constants c_1, c_2, c_3 have profound effect on microrotation as compared to their effect on streamwise and axial velocity profiles. The results of micropolar fluids are compared with the results for Newtonian fluids.

Keywords Porous disks · Asymmetric flow · Micropolar fluid · Finite differences · Viscous layer

M. Ashraf (✉) · M. Anwar Kamal · K. S. Syed
Centre for Advanced Studies in Pure and Applied Mathematics, Bahauddin Zakariya University, Multan, Pakistan
e-mail: mashraf_mul@yahoo.com

M. Anwar Kamal
Department of Mathematics, King Saud University, Riyadh, Saudi Arabia

1 Introduction

The Navier–Stokes model of classical hydrodynamics is inadequate to describe some modern engineering structures which are often made up of materials possessing an internal structure. Polycrystalline materials, fluids containing additives and the materials with fibrous or coarse grain structure fall in this category. The presence of a small amount of additives in the fluid significantly lower down the skin friction near a rigid body and also the frictional drag is reduced by polymer concentration [1]. The classical continua fail to accurately predict the physical nature of asymmetric deformation of these materials. The theory of micropolar fluids introduced by Eringen [2,3] is one of the best theories of fluids to describe the deformation of such materials. Polymeric suspensions, biological fluids, liquid crystals with rigid molecules, muddy fluids, and nemotogenic and smectogenic liquid crystals are some examples of such fluids. Physically these fluids may represent the fluids consisting of rigid randomly oriented particles suspended in a viscous medium undergoing both translational and rotational motion. These fluids can support stress moments and body couples and are influenced by the spin inertia. The stress tensor is not symmetric for such fluids. These fluids represent a good mathematical model for many natural and industrial fluids. The applications of these fluids are in blood flow, lubricants, porous media, turbulent shear flows, and flow in capillaries and micro channels.

The problem of disk flows has constituted a major field of study in fluid mechanics. These flows have applications in the fields of rotating machinery, computer storage devices, heat and mass exchangers, viscometry, lubrication, crystal growth processes, biomechanics and oceanography. Elcrat [4] proved the theorem of existence and uniqueness for non-rotational fluid motion between fixed porous disks with arbitrary uniform injection or suction. The steady viscous flow

between two porous disks was studied by Rasmussen [5]. The fluid motion was symmetrically driven by equal injection or suction at both the disks. Guar et al. [6] solved the problem of temperature distribution and heat transfer for laminar flow through two parallel porous disks with different permeability. The fluid motion was induced due to different injection/suction velocities at the two disks. The steady flow and heat transfer of a conducting fluid due to the rotation of an infinite, non-conducting, porous disk in the presence of an axial uniform steady magnetic field were studied by Attia [7] considering the ion slip. The fluid motion was subjected to the uniform suction or injection through the surface of the porous disk. The transformed non-linear differential equations were solved numerically using an algorithm based on the finite differences.

The steady incompressible flow of a micropolar fluid between a rotating and a stationary disk was described by Guram and Anwar [8]. The problem of steady, laminar and incompressible flow of a micropolar fluid due to a rotating disk was investigated by Guram and Anwar [9]. The flow was driven with uniform suction and injection at the surface of the disk. A comparison of the results of micropolar and Newtonian fluids was also given. The numerical investigations of symmetric flow of micropolar fluid between two porous coaxial disks were considered by Anwar Kamal et al. [10]. Ye et al. [11] considered the problem of laminar flow of micropolar fluids in rectangular microchannels to discuss the micropolar effects on the velocity and microrotation gyration using Chebyshev collocation method. A numerical study of the non-Newtonian behavior of journal bearings lubricated with micropolar fluid was analyzed by Wang et al. [12] by considering both thermal and cavitating effects.

In the present work, we consider the two-dimensional steady, laminar and incompressible flow of a micropolar fluid between two stationary coaxial porous disks. The two disks are of different permeability. The flow is asymmetrically driven by different injection velocities at the two disks. We neglect the effects of body force and body couple.

2 Basic analysis

For the problem under consideration, the suitable coordinate system will be the cylindrical polar coordinate system. Consider two stationary porous disks of radii assumed to be infinite, located in the $Z = -L$ and $Z = L$ planes, respectively, and let the centres of the disks coincide with the axis $r = 0$ as shown in Fig. 1. The domain of the problem is thus the semi-infinite strip in the rz-plane defined by $[0, \infty) \times [-L, L]$.

The velocity components u and w are taken to be in the direction of r-axes and z-axes, respectively.

Fluid is injected through the disks at $Z = -L$ and $Z = L$ with constant velocities V_1 and V_2, respectively. In order to

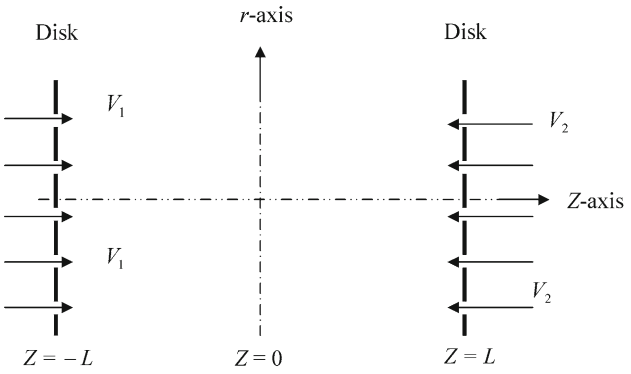

Fig. 1 Geometry of porous disks

investigate the influence of different permeabilities of the porous disks, we define the following permeability parameter.

$$A = 1 - V_1/V_2.$$

The governing equations of motion for the micropolar fluid given by Eringen [2] are as follows

$$\partial\rho/\partial t + \nabla\cdot(\rho \boldsymbol{V}) = 0, \tag{1}$$

$$(\lambda + 2\mu + \kappa)\nabla(\nabla\cdot\boldsymbol{V}) - (\mu+\kappa)\nabla\times\nabla\times\boldsymbol{V} + \kappa\nabla\times\boldsymbol{v} - \nabla\pi + \rho\boldsymbol{f} = \rho\dot{\boldsymbol{V}}, \tag{2}$$

$$(\alpha+\beta+\gamma)\nabla(\nabla\cdot\boldsymbol{v}) - \gamma(\nabla\times\nabla\times\boldsymbol{v}) + \kappa\nabla\times\boldsymbol{V} - 2\kappa\boldsymbol{v} + \rho\boldsymbol{l} = \rho j\dot{\boldsymbol{v}}, \tag{3}$$

where $\boldsymbol{V}$ is the fluid velocity vector, $\boldsymbol{v}$ the microrotation, ρ the density, π the pressure, $\boldsymbol{f}$ and $\boldsymbol{l}$ are body force and body couple per unit mass, respectively, j is the microinertia, λ, μ, α, β, γ, κ are the material constants (or viscosity coefficients) characterizing the microstructure of the micropolar fluids, where dot signifies material derivative.

For the problem under consideration the velocity and the microrotation fields have the general form

$$\boldsymbol{V} = (u(r,z), 0, w(r,z)),$$
$$\boldsymbol{v} = (0, \Phi(r,z), 0). \tag{4}$$

Using these field variables in Eqs. (1)–(3), we find

$$(\mu+\kappa)(\partial^2u/\partial r^2 + (1/r)\partial u/\partial r - u/r^2 + \partial^2u/\partial z^2) - \kappa\partial\Phi/\partial z - \partial\pi/\partial r = \rho(u\partial u/\partial r + w\partial u/\partial z), \tag{5}$$

$$(\mu+\kappa)(\partial^2w/\partial r^2 + (1/r)\partial w/\partial r + \partial^2w/\partial z^2) + \kappa(\partial\phi/\partial r + \phi/r) - \partial\pi/\partial z = \rho(u\partial w/\partial r + w\partial w/\partial z), \tag{6}$$

$$\gamma(\partial^2\phi/\partial r^2 + (1/r)\partial\phi/\partial r - \phi/r^2 + \partial^2\phi/\partial z^2) + \kappa(\partial u/\partial z - \partial w/\partial r) - 2\kappa\phi = \rho j(u\partial\phi/\partial r + w\partial\phi/\partial z), \tag{7}$$

$$\partial u/\partial r + u/r + \partial w/\partial z = 0. \tag{8}$$

The boundary conditions on the disks include specification of the injection velocities (i.e. axial velocity component w), no slip condition (i.e. zero radial velocity u) and zero microrotation. They may be expressed as

$$\begin{aligned} &w(r,-L)=2V_1, \quad && w(r,L)=2V_2,\\ &u(r,-L)=0, && u(r,L)=0,\\ &\phi(r,-L)=0, && \phi(r,L)=0, \end{aligned} \tag{9}$$

where V_1 and V_2 are the uniform injection velocities at the lower and upper disks, respectively.

We have to solve the Eqs. (5)–(8) subject to the boundary conditions (9). For this we use the following similarity transformation similar to that of von Karman [13].

$$u=-rF'(Z), \quad w=2F(Z), \quad \phi=-rG(Z). \tag{10}$$

If we substitute Eq. (10) into Eq. (8), we see that the equation of continuity is identically satisfied and so the velocity components represent the possible fluid motion. By substituting Eq. (10) into Eqs. (5) and (6) we get, after some simplification and elimination of pressure term, the following equation

$$(\mu+\kappa)F^{(iv)}-\kappa G''-2\rho FF'''=0, \tag{11}$$

where

$$\partial^2\pi/\partial r\partial z=0. \tag{12}$$

Again substitute Eq. (10) into Eq. (7), we have

$$\gamma G''+\kappa F''-2\kappa G-\rho j(F'G-2FG')=0. \tag{13}$$

Now dimensionless variables may be defined as

$$f(\eta)=F(Z)/V, \quad g(\eta)=L^2G(Z)/V, \tag{14}$$

where $\eta=Z/L$ and V is the larger of V_1 and V_2.

Substituting Eq. (14) into Eqs. (11) and (13), we shall find

$$f^{(iv)}-c_1g''-2Reff'''=0, \tag{15}$$

$$g'+c_2(f''-2g)-c_3(f'g-2fg')=0, \tag{16}$$

where $Re=\rho VL/(\mu+\kappa)$ is the Reynolds number and

$$c_1=\kappa/(\mu+\kappa), \quad c_2=\kappa L^2/\gamma, \quad c_3=\rho jLV/\gamma$$

are dimensionless micropolar material constants characterizing the vortex viscosity, the spin gradient viscosity and the microinertia density respectively. For $Re<0$ we take the injection at the two disks and for $Re>0$ the problem corresponds to the suction at both the disks. For our problem we use $Re<0$.

Integrating Eq. (15) with respect to η we get

$$f'''-c_1g'-2Reff''+Ref'^2=B, \tag{17}$$

where B is constant of integration and is known as pressure constant.

Substituting Eq. (14) into Eqs. (9) the boundary conditions reduce to

$$\begin{aligned} &f(-1)=1-A, \quad && f(1)=1,\\ &f'(-1)=0, && f'(1)=0,\\ &g(-1)=0, && g(1)=0. \end{aligned} \tag{18}$$

We have to solve Eqs. (16) and (17) subject to the boundary conditions Eqs. (18). We note that Eqs. (16) and (17) reduce to the corresponding equation for a Newtonian fluid for vanishing microrotation and $\kappa=0$.

3 Numerical solution

The governing Eqs. (16) and (17) being highly non-linear cannot be solved analytically. We use a finite difference based numerical algorithm to solve this coupled pair of equations. It is better to reduce the order of Eq. (17) by one with the help of the substitution $p=f'$ so that the boundary value problem consisting of Eqs. (16) and (17) and the boundary conditions Eqs. (18) takes the following form.

Solve

$$p=f'=\mathrm{d}f/\mathrm{d}\eta, \tag{19}$$

$$p''-c_1g'-2Refp'+Rep^2=B \tag{20}$$

$$g''+c_2(p'-2g)-c_3(pg-2fg')=0, \tag{21}$$

subject to the boundary conditions

$$\begin{aligned} &f(-1)=1-A, \quad && f(1)=1,\\ &p(-1)=0, && p(1)=0,\\ &g(-1)=0, && g(1)=0. \end{aligned} \tag{22}$$

For the numerical solution of the above problem we first discretize the domain $[-1, 1]$ uniformly with step h. The solution procedure may be described as follows. Equation (19) is integrated using Simpson's rule [14] with the formula given in Ref. [15]. Equations (20) and (21) are discretized at a typical grid point $\eta=\eta_n$ of the interval $[-1, 1]$ by employing central difference approximations for the derivatives. This results in the following difference equations

$$\begin{aligned} &(2Reh^2p_n-4)p_n+(2-2Rehf_n)p_{n+1}\\ &\quad+(2+2Rehf_n)p_{n-1}=2h^2B+c_1h(g_{n+1}-g_{n-1}) \end{aligned} \tag{23}$$

$$\begin{aligned} &(4+4c_2h^2+2c_3h^2p_n)g_n=(2+2c_3hf_n)g_{n+1}\\ &\quad+(2-2c_3hf_n)g_{n-1}+c_2h(p_{n+1}-p_{n-1}), \end{aligned} \tag{24}$$

where h represents the grid length, $f_n\approx f(\eta_n)$, $p_n\approx p(\eta_n)$ and $g_n\approx g(\eta_n)$.

The algebraic system of equations represented by the above equations is solved iteratively by SOR method [16], subject to the appropriate boundary conditions (22).

We use the following solution procedure which is mainly based on the algorithm described in Ref. [17] in order to

accelerate the iterative procedure, to improve the accuracy of the solution and to have an estimate of local as well as global discretization errors.

For a suitable choice of the values of the grid size h and the relaxation parameter ω, an iterative procedure is started with some initial guess for the values of the constant of integration B and the solution vectors p, g and f, where the kth iteration performs the following steps:

(1) Next approximation for the solution of Eqs. (23) and (24), $p^{(k+1)}$ and $g^{(k+1)}$, respectively, is generated by SOR method subject to the last four conditions in Eqs. (22) for the problem discussed.
(2) New approximation for the solution of Eq. (19), $f^{(k+1)}$, is computed by Simpson's rule subject to the first boundary condition given in Eqs. (22), where $p^{(k+1)}$ is employed for p in Eq. (24).
(3) $p^{(k+1)}$, $g^{(k+1)}$ and $f^{(k+1)}$ are compared with $p^{(k)}$, $g^{(k)}$ and $f^{(k)}$, respectively, to test for convergence.

The iterative procedure is stopped if the following criteria are satisfied for three consecutive iterations

$$\|p^{(k+1)} - p^{(k)}\|_{L_2} < \mathrm{TOL}_{\mathrm{iter}}, \tag{25}$$
$$\|f^{(k+1)} - f^{(k)}\|_{L_2} < \mathrm{TOL}_{\mathrm{iter}}, \tag{26}$$
$$\|g^{(k+1)} - g^{(k)}\|_{L_2} < \mathrm{TOL}_{\mathrm{iter}}. \tag{27}$$

In order to determine the constant of integration B we use hit and trial method by requiring that the computed value of f at the upper boundary $\eta = 1$ matches with the given boundary value of f up to a specified tolerance $\mathrm{TOL}_{\mathrm{iter}}$.

To increase the order of accuracy, the discrete problem is first solved on a basic grid, say $h \in [0, H]$ for $H > 0$. A sequence of approximate solutions is then computed on successively refined grids. Let $U(h_l)$ denotes the discrete solution corresponding to the step sizes

$$h_l = \frac{H}{n_l}, \quad l = 1, 2, 3, \ldots,$$

where $U(h_l)$ stands for either of p and f, $\{n_l\}$ is a sequence of integers associated with the step size sequence $\{h_l\}$ to govern the successive refinement procedure. There are several choices for the sequence $\{n_l\}$ found in literature. We use the Romberg sequence given below

$$S_R = \{1, 2, 4, 8, 16, 32, 64, 128, 256, 512, 1024\}.$$

On the basis of solutions $U(h_l)$, higher order approximations to the exact solutions can be obtained by the use of Richardson's extrapolation. This process can be carried out using any extrapolation scheme [18], e.g. polynomial extrapolation (Aitken–Neville algorithm) or rational extrapolation (Stoer's algorithm). We use polynomial extrapolation, which can be presented as

$$U_{l,1} = U(h_l), \quad l = 1, 2, 3, \ldots, \tag{28}$$
$$U_{l,m} = U_{l,m-1} + \frac{U_{l,m-1} - U_{l-1,m-1}}{(n_l/n_{l-m+1})^2 - 1}, \quad m = 2, 3, \ldots, l, \quad l \geq 2, \tag{29}$$

where l indicates the grid level and m is the number of extrapolation steps. The order of approximation of the solution $U_{l,m}$ increases in even multiples of m, i.e. the error of $U_{m,m}$ is proportional to H^{2m}.

An element of multigrid methods called nested iterations has been used to a limited extent to obtain an improved initial guess for the solution $U^{(l)}$, where $l > 1$, so that rapid convergence of the iterative procedure may be achieved. This may be done by subjecting the solution $U^{(l-1)}$ to an appropriate interpolation operator so that interpolated values are provided at the new grid points of the level l. A computationally convenient choice is the linear operator which gives the improved initial guess for the solution $U^{(l)}$ as follows

$$U_{2i}^{(l)} = U_i^{(l-1)},$$
$$U_{2i+1}^{(l)} = \frac{1}{2}(U_i^{(l-1)} + U_{i+1}^{(l-1)}),$$

where $0 \leq i \leq n_{l-1}N - 1$, and l denotes the grid level.

4 Results and discussion

This section is devoted for the presentation of our findings in tabular and graphical form together with the discussion and their interpretations. As our objective is to develop a better understanding of the effects of micropolar structure of fluids and permeability of two disks on the flow characteristics, we choose to present shear stresses at the two disks, and the velocity and microrotation fields across the disks for a range of values of the Reynolds number Re and a few cases of material properties of micropolar fluids. All the cases of material properties considered in the present work are shown in Table 1 below.

In order to establish the validity of our numerical computations and to improve the order of accuracy of the solutions, numerical results are computed for three grid sizes $h = 0.01, 0.005$ and 0.0025 and then extrapolated using Richardson's extrapolation. The comparison of numerical values of

Table 1 Three cases of micropolar material constants for $Re = -15$ and $A = 1.8$

Case	c_1	c_2	c_3
1	1.0	1.5	2.0
2	5.0	5.5	6.0
3	9.0	9.5	10.0

Table 2 Radial velocity $f'(\eta)$ and its extrapolated values for $Re = -25$, $A = 1.6$, $c_1 = 5.1$, $c_2 = 6.1$ and $c_3 = 7.1$

η	$f'(\eta)$			
	$h = 0.01$	$h = 0.005$	$h = 0.0025$	Extrapolated value
−0.8	0.834618	0.834639	0.834646	0.834649
−0.4	2.548868	2.548594	2.548532	2.548512
0.0	2.646349	2.646273	2.646255	2.646250
0.4	1.558478	1.558577	1.558602	1.558611
0.8	0.515921	0.515950	0.515957	0.515960

Table 3 Axial velocity $f(\eta)$ and its extrapolated values for $Re = -25$, $A = 1.6$, $c_1 = 5.1$, $c_2 = 6.1$ and $c_3 = 7.1$

η	$f(\eta)$			
	$h = 0.01$	$h = 0.005$	$h = 0.0025$	Extrapolated value
−0.8	−0.558522	−0.558521	−0.558521	−0.558520
−0.4	−0.217554	−0.217571	−0.217574	−0.217575
0.0	0.346992	0.346928	0.346914	0.346909
0.4	0.767227	0.767178	0.767167	0.767164
0.8	0.974284	0.974246	0.974239	0.974237

Table 4 Microrotation $g(\eta)$ and its extrapolated values for $Re = -25$, $A = 1.6$, $c_1 = 5.1$, $c_2 = 6.1$ and $c_3 = 7.1$

η	$g(\eta)$			
	$h = 0.01$	$h = 0.005$	$h = 0.0025$	Extrapolated value
−0.8	0.405613	0.405555	0.405541	0.405537
−0.4	0.491803	0.491819	0.491822	0.491823
0.0	−0.420841	−0.420730	−0.420704	−0.420695
0.4	−0.519429	−0.519386	−0.519375	−0.519371
0.8	−0.199743	−0.199752	−0.199754	−0.199755

streamwise velocity, axial velocity and the microrotation for the three grid sizes and their extrapolated values are given in Tables 2, 3 and 4, respectively. Excellent comparison validates our numerical computation and the use of extrapolation to improve the accuracy of the results.

In order to facilitate understanding of the influence of the permeability parameter A and the Reynolds number Re on the flow fields, we first note that A is determined by the ratio of the injection velocities at the two disks and Re is based on the injection velocity at the upper disk. When $Re = 0$, the problem becomes that of the flow with impermeable disks. In such a case A will be arbitrary and have no effect on the flow in view of the relation $V_1 = (1 - A)V_2$ (by definition of A given in the Sect. 2), where $V_1 = 0 = V_2$. When the magnitude of Re is increased for a fixed value of A, it corresponds to the situation in which the injection velocities at the upper and lower disks are increased keeping their ratio constant. On the other hand if Re is fixed and A is increased from 1 to 2, it represents the situation in which, for a given injection velocity at the upper disk, the injection velocity at the lower disk is increased from zero to the magnitude of that at the upper disk. For $Re < 0$, the case $A = 1$ corresponds to the problem of flow with impermeable lower disk and permeable upper disk, $1 < A < 2$ corresponds to the non zero and unequal injection velocities at the lower and upper disks and $A = 2$ represents the problem of symmetric flow with equal injection velocities at both the disks.

Table 5 Skin friction at lower and upper disks for $Re = -100$, $c_1 = 5.1$, $c_2 = 6.1$, $c_3 = 7.1$ and various A

A	$f''(-1)$	$f''(1)$
1.0	35.8521	−2.1587
1.2	14.0248	−2.9157
1.4	9.5979	−3.9370
1.6	8.4396	−5.1275
1.8	8.0601	−6.4782
2.0	7.9883	−7.9882

First of all we present the influence of permeability parameter A on shear stresses for a fixed value of Re and material constants c_1, c_2 and c_3. As A is increased, the shear stress at the lower disk decreases while it increases at the upper disk. For this case, the shear stress at the lower disk is maximum while it is minimum in magnitude at the upper disk. This is the most asymmetric case. We note from Table 5 that as A is increased from 1 to 2, the shear stress at the lower disk decreases from its maximum value to a minimum value while at the upper disk its magnitude increases from its minimum value to the maximum value so that for $A = 2$, the shear stress at both the disks becomes equal reflecting the symmetry of the problem.

Now in order to investigate the effect of dimensionless constants c_1, c_2, c_3, Re and A on the primary flow fields, we give graphical presentation of the streamwise and axial velocity profiles, and the microrotation across the disks. The influence of the Reynolds number Re on the streamwise velocity is presented in Fig. 2 for fixed values of A, c_1, c_2 and c_3. For $Re = 0$, the profile is symmetric and parabolic with respect to the central plane $Z = 0$. When the non-zero injection velocity V_2 is imposed at the upper disk (i.e. $Re < 0$), for $A = 1.6$ which corresponds to the injection velocity at the lower disk to be 60% of V_2, the profile becomes asymmetric pushed towards the lower disk. As the magnitude of Re is increased, the profile becomes more asymmetric. The point of maximum velocity is shifted towards the lower disk and the streamwise velocity on the lower disk side increases while it decreases on the upper disk side. For large value of Re, the effect of varying Re tends to become insignificant.

Figure 3 presents the profiles of axial velocity component to reflect the influence of Re on its behavior for typical values

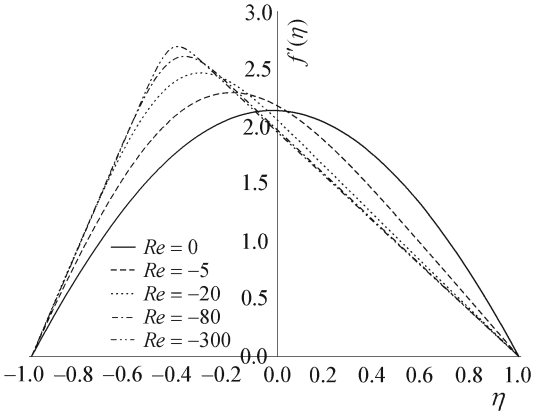

Fig. 2 Radial velocity profiles of micropolar fluids for $A = 1.4$, $c_1 = 2.0$, $c_2 = 2.5$, $c_3 = 3.0$ and various Re

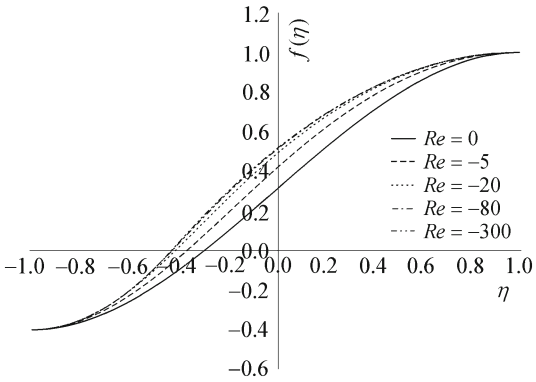

Fig. 3 Axial velocity profiles of micropolar fluids for $A = 1.4$, $c_1 = 2.0$, $c_2 = 2.5$, $c_3 = 3.0$ and various Re

of A and dimensionless constants c_1, c_2 and c_3. The axial velocity takes its dimensionless value –1 at the lower disk and increases to1 at the upper disk with a point of inflection somewhere near the central plane $Z = 0$ where it changes its concavity. As the magnitude of Re is increased, the profiles reflect significant increase in the axial velocity within the region away from the disks for $-50 \leq Re \leq 0$. As Re is further increased in magnitude, its effect becomes less influential and the gaps between the profiles appear to approach zero as $Re \to -\infty$. This is due to the constraints of axial velocity being -1 at the lower disk and 1 at the upper disk, which do not allow the axial velocity to increase indefinitely as the magnitude of Re is increased.

The behavior of the microrotation for fixed values of A, c_1, c_2, c_3 and for different values of the Reynolds number Re is shown graphically in Fig. 4. The shear stresses at the two disks tend to rotate the fluid in opposite directions because of which the microrotation has opposite sign near the disks. When $Re = 0$, the effect of shear stresses propagates at equal rate from the disks resulting into zero microrotation at the central plane $Z = 0$. As the magnitude of Re is increased,

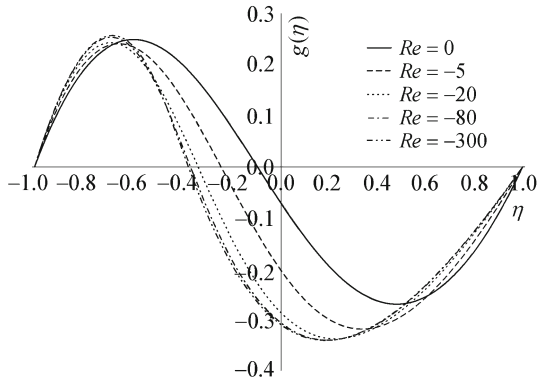

Fig. 4 Microrotation profiles of micropolar fluids for $A = 1.4$, $c_1 = 2.0$, $c_2 = 2.5$, $c_3 = 3.0$ and various Re

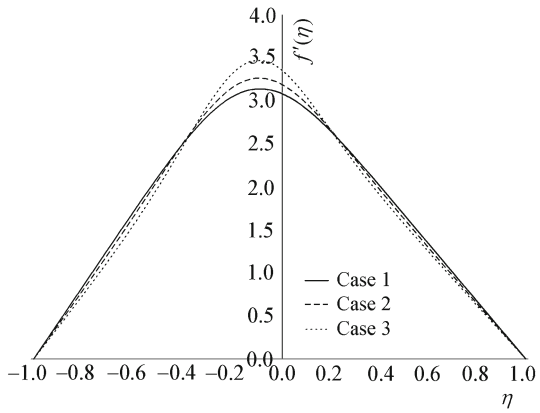

Fig. 5 Radial velocity profiles of micropolar fluids for $Re = -15$, $A = 1.8$ and three cases of micropolar material constants

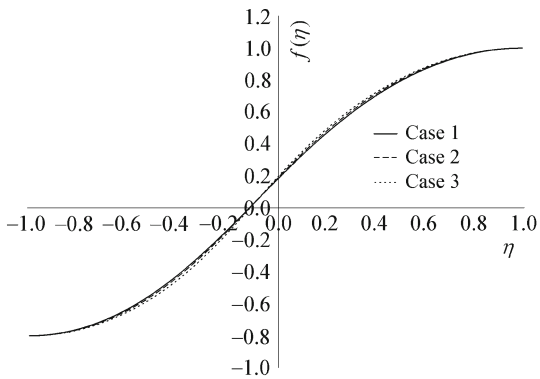

Fig. 6 Axial velocity profiles of micropolar fluids for $Re = -15$, $A = 1.8$ and three cases of micropolar material constants

the microrotation increases, and the point of zero microrotation moves towards the lower disk.

Figures 5, 6 and 7 show streamwise velocity, axial velocity and microrotation profiles for three sets of values of c_1, c_2 and c_3 (given in Table 1) when A and Re are fixed. The values of c_1, c_2 and c_3 have significant effect on microrotation as compared to their effect on streamwise and axial velocity profiles. The maximum value of streamwise velocity and

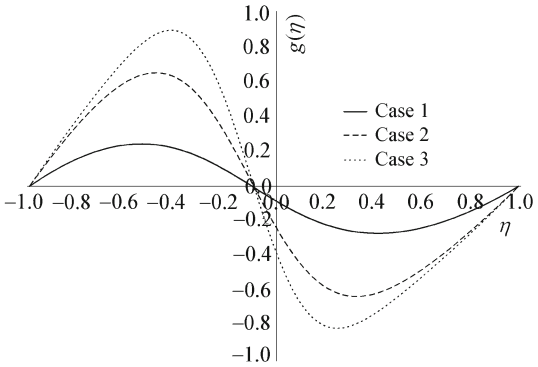

Fig. 7 Microrotation profiles of micropolar fluids for $Re = -15$, $A = 1.8$ and three cases of micropolar material constants

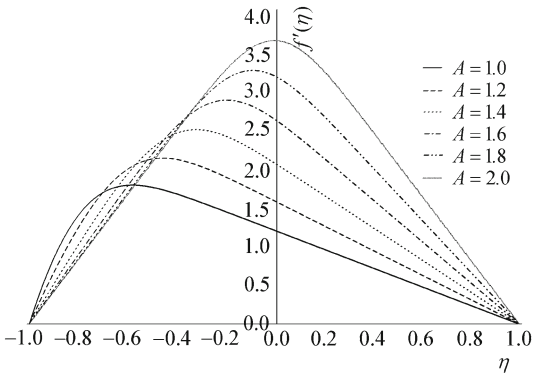

Fig. 8 Radial velocity profiles of micropolar fluids for $Re = -25$ and various A

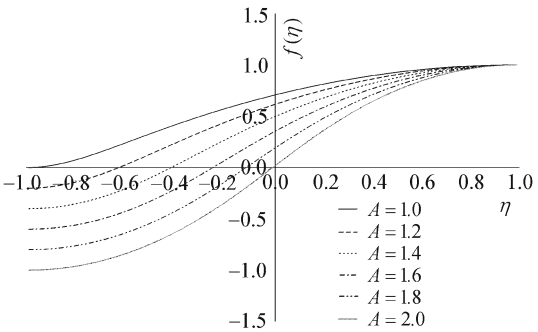

Fig. 9 Axial velocity profiles of micropolar fluids for $Re = -25$ and various A

microrotation increases as we increase the values of c_1, c_2 and c_3.

The effect of A on the velocity and microrotation profiles is shown in Figs. 8, 9 and 10 for fixed values of Re, c_1, c_2 and c_3. The streamwise velocity increases by increasing A across a major part near the upper disk and the profile tends to become symmetric as A is increased from 1 to 2. The maximum value of streamwise velocity increases by increasing A. The axial velocity profiles given in Fig. 9 are helpful in finding the position of viscous layer, which is developed due to the injection at the two disks. The position of viscous

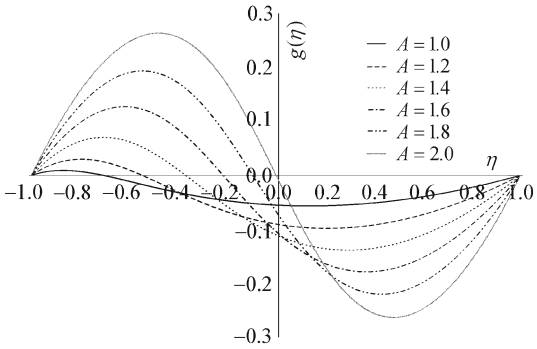

Fig. 10 Spin profiles of micropolar fluids for $Re = -25$ and various A

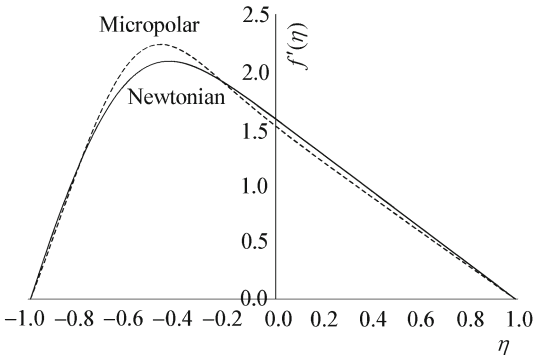

Fig. 11 Comparison of radial velocity profiles of Newtonian and micropolar fluids for $Re = -20$ and $A = 1.2$

layer is a point where $f(\eta) = 0$. We observe from the Fig. 9 that the position of viscous or shear layer moves towards the central plane $Z = 0$ as we increase A. For $A = 2$, this viscous layer coincides with the central plane $Z = 0$ and the problem reduces to the symmetrical injection case, discussed by Ref. [13] for Newtonian fluids. A comparison of Figs. 3 and 9 shows that the position of viscous layer is more sensitive to the permeability parameter A than to the Reynolds number Re. From microrotation profiles shown in Fig. 10, it can be observed that the position of the point where the curves change their concavity goes on shifting towards the central plane $Z = 0$ by increasing A. The maximum value of microrotation increases while the minimum value decreases as A is increased so that they reach their respective extremes at $A = 2$. A comparison of the profiles of streamwise velocity for Newtonian and micropolar fluids shown in Fig. 11 validates our micropolar model.

5 Conclusions

In the present work, we have considered the numerical solution of the problem of two dimensional steady, laminar and incompressible flow of a micropolar fluid between two parallel porous disks of different permeability. The problem of

the flow with one permeable and the other impermeable disk and that of the symmetric flow with both permeable or both impermeable disks occur as special cases of the present problem corresponding to the parametric values $A = 1$ and $Re < 0$, $A = 2$ and $Re < 0$, $Re = 0$ and A arbitrary respectively. The objective of the present study is to investigate the effects of the Reynolds number Re and permeability parameter A, determined by the injection velocities at the two disks, and the material constants on the flow variables. The results indicate that the parameters Re and A have a strong influence on the velocity and microrotation profiles, shear stresses at the disks and the position of the viscous/shear layer. The velocity and microrotation profiles change from the most asymmetric shape to the symmetric shape across the disks as the Reynolds number Re is increased from some negative value to zero or the permeability parameter A is increased from 1 to 2. The shear stress at a disk depends strongly on the injection velocity at it determined by the choice of the values of Re and A. Larger the injection velocity at a disk relative to the other is, smaller will be the shear stress at it than that at the other. The position of viscous layer has been found to be more sensitive to the permeability parameter A than to the Reynolds number Re. The material constants c_1, c_2 and c_3 have profound effect on microrotation as compared to their effect on streamwise and axial velocity profiles. For the fluids with larger values of these material constants, the effect of micropolar structure cannot be ignored.

Acknowledgments The authors are thankful to the editorial board of the journal and the referees for their constructive comments.

References

1. Eringen, A.C.: Theory of micropolar continua. In: Proceedings of the Ninth Midwestern Mechanics Conference, p. 23 (1965)
2. Eringen, A.C.: Simple microfluids. Int. J. Eng. Sci. **2**, 205–217 (1964)
3. Eringen, A.C.: Theory of micropolar fluids. J. Math. Mech. **16**, 1–18 (1966)
4. Elcrat, A.R.: On the radial flow of a viscous fluid between porous disks. Arch. Rat. Mech. Anal. **61**, 91–96 (1976)
5. Rasmussen, H.: Steady viscous flow between two porous disks. Z. Angew. Math. Phys. **21**, 187–195 (1970)
6. Guar, Y.N., Chaudhary, R.C.: Heat transfer for laminar flow through parallel porous disks of different permeability. Proc. Indian Acad. Sci. **87A**, 209–217 (1978)
7. Attia, H.A.: On the effectiveness of the ion slip on the steady flow of a conducting fluid due to a porous rotating disk with heat transfer. Tamkang J. Sci. Eng. **9**(3), 185–193 (2006)
8. Guram, G.S., Anwar, M.: Steady flow of a micropolar fluid due to a rotating disk. J. Eng. Math. **22**, 467–485 (1979)
9. Guram, G.S., Anwar, M.: Micropolar flow due to a rotating disc with suction and injection. ZAMM **61**, 589–605 (1981)
10. Anwar Kamal, M., Ashraf, M., Syed, K.S.: Numerical solution of steady viscous flow of a micropolar fluid driven by injection between two porous disks. Appl. Math. Comput. **179**, 1–10 (2006)
11. Ye, S.J., Zhu, K.Q., Wang, W.: Laminar flow of micropolar fluid in rectangular microchannels. Acta Mech. Sin. **22**, 403–408 (2006)
12. Wang, X.L., Zhu, K.Q.: Numerical analysis of journal bearings lubricated with micropolar fluids including thermal and cavitating effects. Tribol. Int. **39**, 227–237 (2006)
13. von Karman, T.: Under laminare and turbulente Reibung. Z. Angew. Math. Mech. **1**, 233–235 (1921)
14. Gerald, C.F.: Applied Numerical Analysis. Addison-Wesley, Reading (1974)
15. Milne, W.E.: Numerical Solutions of Differential Equations. Wiley, New York (1953)
16. Hildebrand, F.B.: Introduction to Numerical Analysis. McGraw-Hill, New York (1978)
17. Syed, K.S., Tupholme, G.E., Wood, A.S.: Iterative solution of fluid flow in finned tubes. In: Taylor, C., Cross, J.T. (eds.) Proceedings of the 10th International Conference on Numerical Methods in Laminar and Turbulent Flow, vol. 21–25, pp. 429–440. Pineridge Press, Swansea (1997)
18. Deuflhard, P.: Order and step-size control in extrapolation methods. Numer. Math. **41**, 399–422 (1983)